1950 *Biochemistry* **2011,** *50,* 1950–1962
DOI: 10.1021/bi101927s

BIOCHEMISTRY
including biophysical chemistry & molecular biology
Article

Mechanistic Studies of 1-Aminocyclopropane-1-carboxylate Deaminase: Characterization of an Unusual Pyridoxal 5′-Phosphate-Dependent Reaction†

Christopher J. Thibodeaux and Hung-wen Liu*

Division of Medicinal Chemistry, College of Pharmacy, Department of Chemistry and Biochemistry, and Institute for Cellular and Molecular Biology, University of Texas, Austin, Texas 78712, United States

Received December 2, 2010; Revised Manuscript Received January 17, 2011

ABSTRACT: 1-Aminocyclopropane-1-carboxylic acid (ACC) deaminase (ACCD) is a pyridoxal 5′-phosphate (PLP)-dependent enzyme that cleaves the cyclopropane ring of ACC, to give α-ketobutyric acid and ammonia as products. The cleavage of the $C_\alpha-C_\beta$ bond of an amino acid substrate is a rare event in PLP-dependent enzyme catalysis. Potential chemical mechanisms involving nucleophile- or acid-catalyzed cyclopropane ring opening have been proposed for the unusual transformation catalyzed by ACCD, but the actual mode of cyclopropane ring cleavage remains obscure. In this report, we aim to elucidate the mechanistic features of ACCD catalysis by investigating the kinetic properties of ACCD from *Pseudomonas* sp. ACP and several of its mutant enzymes. Our studies suggest that the pK_a of the conserved active site residue, Tyr294, is lowered by a hydrogen bonding interaction with a second conserved residue, Tyr268. This allows Tyr294 to deprotonate the incoming amino group of ACC to initiate the aldimine exchange reaction between ACC and the PLP coenzyme and also likely helps to activate Tyr294 for a role as a nucleophile to attack and cleave the cyclopropane ring of the substrate. In addition, solvent kinetic isotope effect (KIE), proton inventory, and ^{13}C KIE studies of the wild type enzyme suggest that the $C_\alpha-C_\beta$ bond cleavage step in the chemical mechanism is at least partially rate-limiting under k_{cat}/K_m conditions and is likely preceded in the mechanism by a partially rate-limiting step involving the conversion of a stable *gem*-diamine intermediate into a reactive external aldimine intermediate that is poised for cyclopropane ring cleavage. When viewed within the context of previous mechanistic and structural studies of ACCD enzymes, our studies are most consistent with a mode of cyclopropane ring cleavage involving nucleophilic catalysis by Tyr294.

1-Aminocyclopropane-1-carboxylate deaminase (ACCD)[1] is a pyridoxal 5′-phosphate (PLP)-dependent enzyme expressed in certain soil bacteria and fungi that catalyzes the conversion of 1-aminocyclopropane-1-carboxylic acid (ACC, **1**) to α-ketobutyrate (α-KB, **2**) and ammonia (Scheme 1) (*1*). In plants, ACC is the immediate biosynthetic precursor to ethylene, an important plant hormone that regulates fruit ripening, seed germination, leaf senescence, responses to environmental stress, and many other physiological events (*2*). In the soil-dwelling organisms that express ACCD, the function of ACCD may be to salvage useful sources of carbon and nitrogen for metabolic needs. Bacterial ACCDs have been incorporated into transgenic plants to regulate ethylene biosynthesis, and ACCD expression in plant tissues can lead to significant delays in fruit ripening, helping to increase the shelf life of fruits and vegetables (*3*).

Scheme 1: Reaction Catalyzed by ACC Deaminase

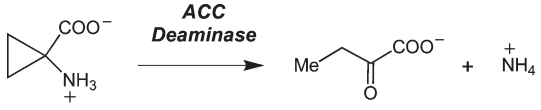

ACC (**1**) α-ketobutyric acid (**2**)

The catalytic cycles of most PLP-dependent enzymes begin with the formation of an external aldimine (such as **4** in Scheme 2) between the amino group of the substrate and the PLP coenzyme (*4*−*6*). In the vast majority of PLP-dependent enzymes, a C_α anion species (such as **5**) is then generated either by the deprotonation of the $C_\alpha-H$ bond or by decarboxylation of the α-carboxyl group of the substrate. In this respect, the reaction catalyzed by ACCD is unusual, because the amino acid substrate, ACC, contains no C_α proton and the carboxylate group is retained in the α-KB product. In ACCD, the C_α anion equivalent could be generated by cleavage of one of the two $C_\alpha-C_\beta$ bonds of ACC. However, $C_\alpha-C_\beta$ bond cleavage is a rare event in PLP-dependent enzyme catalysis and has been observed in only one other enzyme, serine hydroxymethyltransferase (SHMTase) (*7*, *8*). In this enzyme, the $C_\alpha-C_\beta$ bond of the serine−PLP external aldimine is believed to be cleaved either by a retro-aldol type reaction or as a result of direct nucleophilic attack by the

†This work was supported in part by a grant from the National Institutes of Health (GM040541) and a fellowship from the Graduate School of the University of Texas to C.J.T.

*To whom correspondence should be addressed. Phone: (512) 232-7811. Fax: (512) 471-2746. E-mail: h.w.liu@mail.utexas.edu.

[1]Abbreviations: α-KB, 2-keto-1-butanoic acid; ACC, 1-aminocyclopropane-1-carboxylic acid; ACCD, 1-aminocyclopropane-1-carboxylate deaminase; ACP, 1-aminocyclopropane 1-phosphonate; CAPSO, 3-(cyclohexylamino)-2-hydroxy-1-propanesulfonic acid; EPPS, 4-(2-hydroxyethyl)-1-piperazinepropanesulfonic acid; HMP, 4-hydroxyl-*N*-methylpiperidine; HEPES, 4-(2-hydroxyethyl)-1-piperazineethanesulfonic acid; KIE, kinetic isotope effect; LDH, L-lactate dehydrogenase; MES, 2-(*N*-morpholino)ethanesulfonic acid; MOPS, 3-(*N*-morpholino)propanesulfonic acid; MSR, mean-square residual of the fit; NADH, nicotinamide adenine dinucleotide (reduced form); NMR, nuclear magnetic resonance; PLP, pyridoxal 5′-phosphate; SHMTase, serine hydroxymethyltransferase; TAPS, *N*-tris(hydroxymethyl)methyl-3-aminopropanesulfonic acid; wt, wild type.

 Published on Web 01/18/2011

Scheme 2: Putative Chemical Mechanisms for ACCD Involving Nucleophile- and Base-Catalyzed Ring Scission (paths A and B, respectively)

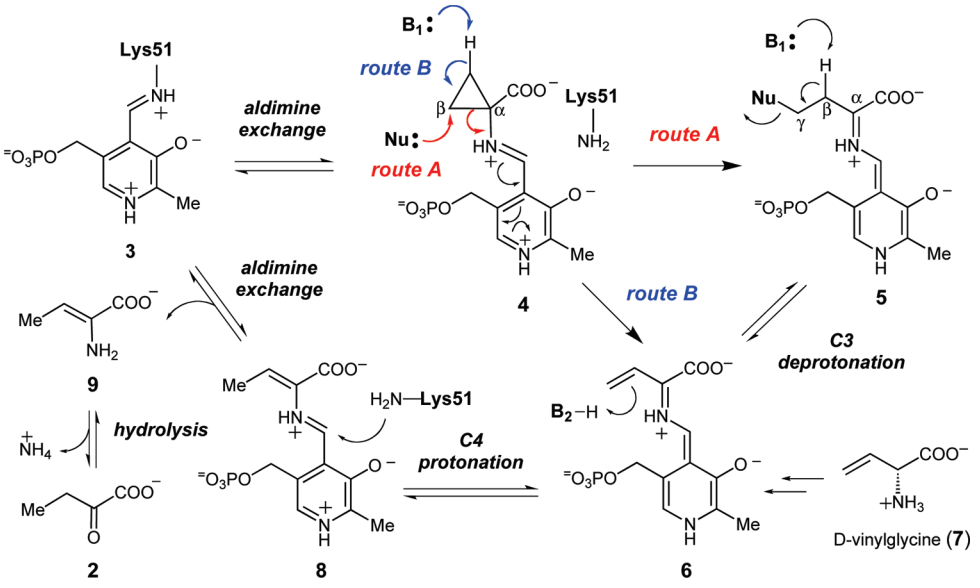

tetrahydrofolate cosubstrate on the C_β atom of the serine substrate.

Several possible mechanisms can be envisioned for the $C_\alpha-C_\beta$ bond cleavage event catalyzed by ACCD (*9*). As shown in route A in Scheme 2, following conversion of the internal aldimine (**3**) to the ACC−PLP−external aldimine complex (**4**), an active site nucleophile could attack and trigger the cleavage of the ACC cyclopropane ring (*10*, *11*) to yield the C_α anion equivalent (or quinonoid, **5**). This mechanism is conceivable because cyclopropane rings bearing electron-withdrawing substituents are known to be susceptible to nucleophilic addition reactions (*12*−*15*). Removal of a proton at C_β of the quinonoid (**5**) (*9*, *16*) by an active site base (B_1) could then eliminate the nucleophile to afford the vinylglycyl-PLP quinonoid intermediate (**6**). Support for the intermediacy of **6** in the catalytic cycle of ACCD is derived from mechanistic studies with D-vinylglycine (**7**, Scheme 2), which can also be converted to α-KB (**2**) and ammonia by ACCD (*9*). Subsequent C_γ protonation of **6** by a separate active site residue (B_2) (*16*) could give the PLP−aminocrotonate species (**8**). Aldimine exchange and hydrolysis of **9** could then regenerate the internal aldimine (**3**) and yield the reaction products, α-KB (**2**) and ammonia. A variety of stereochemical studies have suggested that the $C_\beta-C_\alpha$ bond cleavage is *pro-S* stereospecific (*10*), that C_β deprotonation (**5** → **6**, *pro-R* dominant) and protonation (**9** → **2**, *pro-R* dominant) are mediated by a single base (B_1), and that both B_1 and B_2 are located on the *si* face of the alkene moiety of **6** (*16*). A second potential mechanism that has been proposed for the ACC ring scission step involves deprotonation of one of the two C_β-methylene carbons of the ACC−PLP−external aldimine complex (**4**) to generate the extended quinonoid intermediate (**6**) directly (Scheme 2, route B) (*9*). However, the pK_a of ~46 for the ring hydrogens of cyclopropane (*17*) seems prohibitively high for this mechanism to be feasible.

The X-ray crystal structures of ACCD enzymes from both yeast and bacterial sources have been reported previously (*18*−*21*) and, together with the stereochemical studies discussed above (*9*, *10*, *16*), have provided important insight into the putative roles of several active site amino acid residues in the ACCD-catalyzed reaction. Specifically, the phenoxyl side chain of Tyr294 (*Pseudomonas* sp. ACP numbering) is located only 3 Å from the *pro-S* C_β of the ACC cyclopropane ring (Figure 1). As such, it appears to be positioned appropriately to serve as a nucleophile to attack the *pro-S* C_β and cleave the *pro-S* $C_\beta-C_\alpha$ bond of the ACC cyclopropane ring. In support of this proposed catalytic role, the Y294F mutant is completely inactive, and no consumption of ACC was detected by ^{1}H NMR spectroscopy after a 24 h incubation period (*20*). A putative hydrogen bonding interaction between Tyr268 and Tyr294 (2.5 Å) could lower the pK_a of Tyr294, enhancing its role as a catalytic nucleophile. Ser78 is also located close to the ACC−PLP adduct in the active site, where it forms a hydrogen bond with the carboxylate group of ACC (2.8 Å) and could help mediate proton transfers during turnover (*22*). Finally, Glu295 appears to form an ion pair interaction with the pyridinium group of PLP. Such interactions are common in PLP enzymes and are generally believed to increase the pK_a of the pyridine ring to maximize the electrophilic properties of the coenzyme.

An unusual feature of the wild type (wt) ACCD−ACC cocrystal structure is the apparent accumulation of a *gem*-diamine species (**10**, Scheme 3) in the active site, where the amino groups of ACC and the Schiff base-forming lysine residue (Lys51) are both covalently linked to the C4′ atom of the coenzyme (Figure 1) (*20*, *21*). In most PLP-dependent enzymes, the *gem*-diamine is a transient species during the aldimine exchange reaction (see the **3** → **4** reaction in Scheme 2). The observation of this unusual *gem*-diamine species in the wt ACCD−ACC cocrystal structure prompted us to consider an alternative mechanistic possibility for ACCD, in which Tyr294 acts as an active site acid to facilitate the cleavage of the cyclopropane ring directly from the *gem*-diamine intermediate (Scheme 3) (*21*). After formation of the *gem*-diamine intermediate (**10**), a "push" by the electron pair of the ACC amine and a "pull" by the concomitant protonation at the *pro-S* C_β of ACC by Tyr294 could facilitate the cleavage of the $C_\alpha-C_\beta$ bond to generate **11**. Stereospecific C_β deprotonation of **11** could give **12**, and the aldimine exchange reaction could release the aminocrotonate (**9**) and regenerate the internal aldimine (**3**). Subsequent tautomerization of **9** and hydrolysis of the resulting imine would eliminate ammonia to give α-KB (**2**). Although this

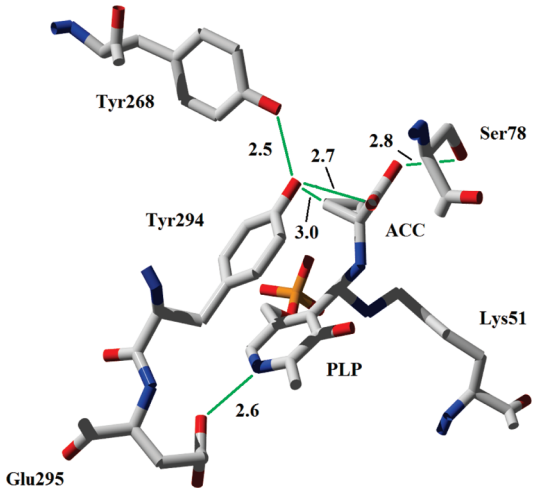

FIGURE 1: Active site of wild type ACCD from *Pseudomonas* sp. ACP in complex with ACC (**1**). Distances are given in angstroms.

proposal represents an unprecedented catalytic cycle for a PLP-dependent enzyme in that the electron sink properties of the coenzyme are not used, it provides a rationale for the accumulation of the *gem*-diamine (**10**) in the wt ACCD−ACC cocrystal structure. Furthermore, the acid-catalyzed electrophilic cleavage of cyclopropanes is well-documented in model studies (*23*−*27*).

In this study, we investigate the kinetic and spectroscopic properties of wt ACCD from *Pseudomonas* sp. ACP and several of its active site mutants in an attempt to distinguish among the possible chemical mechanisms for ACCD catalysis involving either nucleophile or acid-catalyzed cyclopropane ring opening. Kinetic−pH profiles are used to assess the involvement of acid−base chemistry in catalysis and to help define the protonation states of groups that are important to substrate binding and catalysis. Pre-steady state stopped-flow absorption spectroscopy of wt ACCD and its mutants is used to provide insight into the PLP-linked intermediates that form during turnover. Finally, solvent kinetic isotope effects, proton inventory studies, viscosity variation experiments, and ^{13}C KIE studies of the wt enzyme help to define the sequence of chemical events involved in catalysis and to characterize the nature of the steps that limit steady state turnover.

MATERIALS AND METHODS

General. Wild type (wt) ACCD from *Pseudomonas* sp. ACP and its Y268F and Y294F mutants were expressed in *Escherichia coli* as N-His_6 fusion proteins as described previously (*21*). The wt ACCD gene in the pET28b(+) construct (Stratagene, La Jolla, CA) was used as a template to generate the Glu295 → Asp295 mutation using the QuikChange site-directed mutagenesis kit (Amersham, Arlington Heights, IL) with the forward primer (5′-GCTGACCGATCCCGTCTAC**GAT**GGCAAATCGATGCA-CGGCA) and the reverse primer (5′-TGCCGTGCATCGA-TTTGCC**ATC**GTAGACGGGATCGGTCAGC) (mutation in bold). The mutation was confirmed by DNA sequencing performed by the Institute of Cellular and Molecular Biology Core Laboratories of the University of Texas. The E295D protein was expressed and purified in a fashion similar to those of the other enzymes used in this study (*21*). L-Lactic dehydrogenase from rabbit muscle, β-nicotinamide adenine dinucleotide (NADH), ACC (**1**), and all buffer components used in this study were purchased from Sigma-Aldrich (St. Louis, MO). All protein concentrations were determined by the Bradford method using bovine serum albumin as the standard (*28*). All curve fitting was performed with GraFit 5 (Erithacus Software, Horley, Surrey, U.K.).

pH Dependence of the Steady State Kinetic Parameters. Steady state kinetic measurements were taken with a continuous coupled enzyme assay in which the α-KB (**2**) produced by ACCD turnover is reduced with NADH to 2-hydroxybutanoic acid by lactate dehydrogenase (LDH) (*9*, *22*). A typical 500 μL reaction mixture contained 100 units of LDH, 200 μM NADH, 1.68 μM wt ACCD, and variable concentrations of ACC (0.1−50 mM) in assay buffer (25 mM MOPS, 25 mM MES, and 50 mM HMP) adjusted to the appropriate pH with 10 M HCl or 10 M NaOH. After the buffer pH had been adjusted, the final ionic strength was increased to 100 mM by the addition of NaCl. Upon addition of ACC to initiate the reaction, the rate of NADH consumption at 340 nm was monitored (ε_{340} = 6220 M^{-1} cm^{-1}) at 25 °C. For Y268F, E295D, and wt ACCD in D_2O, the concentration of enzyme was increased to 15.4, 4.95, and 3.36 μM, respectively. For assays performed in D_2O, the assay buffer components were mixed directly in D_2O (99.9 at. % D, Sigma-Aldrich) and were adjusted to the appropriate pD (pD = pH meter reading + 0.4) with 10 M HCl or 10 M NaOH. This solution was used to make the NADH, LDH, ACC, and enzyme stock solutions. The final mole fraction of protium in these reaction mixtures was calculated to be < 5%.

The choice of ACC concentrations used depended on the enzyme and the K_m value at the particular pH being assayed, but in all cases, at least three or four different substrate concentrations both above and below the K_m value were used. The initial velocity at each substrate concentration was measured in triplicate, and the substrate concentration dependence of the initial velocities was fit with the Michaelis−Menten equation for the determination of k_{cat} and K_m. The k_{cat} and k_{cat}/K_m values determined at each pH [$k_{cat,app}$ and $(k_{cat}/K_m)_{app}$] were normalized by the enzyme concentration, and the log values of these kinetic constants were plotted versus pH and fit with eqs 1−3. The $\log(k_{cat}/K_m)_{app}$ data were fit with eq 1 or 2, each describing inverse bell-shaped profiles with slopes of +1 and −1 at low and high pH, respectively. In these equations, k_{cat}/K_m is the pH-independent value of k_{cat}/K_m, pK_1 and pK_2 (eq 1) are the apparent pK_a values of titratable groups in the free enzyme and free substrate, respectively, and pK' (in eq 2) is the average of two closely spaced apparent pK_a values. Equation 3 describes a profile that increases to a maximal value (k_{cat}) at high pH with a slope of +1 and the apparent dissociation constant, pK_3.

$$\log(k_{cat}/K_m)_{app} = \log[(k_{cat}/K_m)/(1 + 10^{pK_1 - pH} + 10^{pH - pK_2})] \quad (1)$$

$$\log(k_{cat}/K_m)_{app} = \log[(k_{cat}/K_m)/(2 + 10^{pK' - pH} + 10^{pH - pK'})] \quad (2)$$

$$\log(k_{cat,app}) = \log(k_{cat} + 10^{pK_3 - pH}) \quad (3)$$

Spectrophotometric pH Titrations of the Internal Aldimine. To monitor the pH dependence of the tautomerization between the enolimine and ketoenamine forms of the internal aldimine, enzymes [stored in 50 mM Na_2HPO_4 and 10% glycerol (pH 7.5)] were diluted to 50 μM in 100 mM buffer (specified below), and following a 1 min incubation, the absorbance of each

Scheme 3: Putative Chemical Mechanism for ACCD Involving Acid-Catalyzed Ring Scission

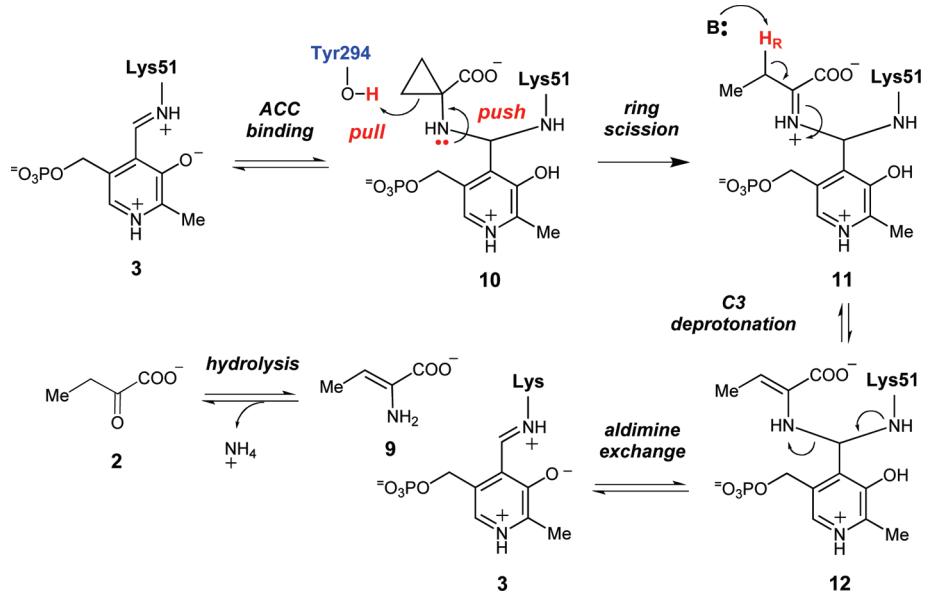

sample was recorded from 200 to 900 nm on a Beckman DU 650 spectrophotometer at 25 °C. The following buffers were used: HEPES (pH 6.8−7.5), EPPS (pH 7.3−8.2), TAPS (pH 8.0−9.0), and CAPSO (pH 9.2−10.2). The spectra were normalized by setting the average absorbance values from 850 to 900 nm to zero.

Viscosity Variation Experiments. Viscosity variation experiments were performed under pseudo-first-order conditions with wt ACCD using glycerol as the viscogen. The reaction mixtures contained 1.2 μM ACCD, 30 mM ACC, and variable concentrations of glycerol [0, 10, 16, 20, 24, 30, and 32% (w/v)] in 25 mM MOPS, 25 mM MES, and 50 mM HMP (pH 7.5) at 25 °C. The coupled LDH reporter assay described above was used to detect the formation of the α-KB product. Each reaction was performed in triplicate, and the dependence of the initial velocity on the relative viscosity of the solution was determined by fitting the data to eq 4

$$k_o/k_\eta = S(\eta_{rel} - 1) + 1 \quad (4)$$

where k_o, k_η, and η_{rel} are the initial velocity in buffer with no added viscogen, the initial velocity in buffer with relative viscosity η, and the relative viscosity of the solution, respectively. The slope of the plot, S, is unity for a reaction that is completely diffusion controlled, zero for a reaction that is not diffusion controlled, and between zero and one for a reaction that is partially diffusion controlled. The relative viscosities of the solutions containing variable concentrations of glycerol were taken from ref *29*.

Proton Inventory Study of wt ACCD. For these studies, the production of α-KB was monitored directly by following the increase in absorbance at 329 nm (ε_{329} = 0.0176 mM^{-1} cm^{-1} for α-KB). The reactions were performed at pL 8.0, where the k_{cat} in both 100% H_2O and 100% D_2O is relatively independent of pL. TAPS buffer (50 mM) was prepared with a 0, 20, 40, 60, 80, or 100% (v/v) D_2O/H_2O mixture. The pL was adjusted to 8.0 using 10 and 1 M solutions of NaOH, and the ionic strength was adjusted to 100 mM with NaCl. In each separate D_2O/H_2O mixture, 10 μL of the wt ACCD stock (in H_2O, 1.19 mM) and 30 μL of a 500 mM ACC solution (dissolved in the appropriate D_2O/H_2O mixture) were added to a total reaction volume of 500 μL, giving wt ACCD and ACC at final concentrations of 23.8 μM and 30 mM, respectively. The mole fraction of deuterium for each water mixture was corrected to account for the different molar volumes of H_2O and D_2O (*30*), and also for solvent exchangeable protons derived from TAPS, NaOH, ACC, and the components of the stock enzyme solution. The enzyme was preincubated in each water mixture for approximately 30 min prior to the addition of ACC to start the reaction. Following a 4 min incubation period, the production of α-KB was monitored over a 4 min period by the increase in A_{329}. Under these conditions, the formation of α-KB was a linear function of time for all reactions. In each water mixture, replicate measurements of the initial velocity were taken under pseudo-first-order substrate concentrations (as an estimate of k_{cat}), and the data were fitted with several different forms of the Gross−Butler equation (eq 5)

$$k_n/k_o = \prod_i^{V_i}(1 - n + n\Phi_{TS})_i / \prod_j^{V_j}(1 - n + n\Phi_R)_j \quad (5)$$

where k_o and k_n are the k_{cat} values in buffers of deuterium atom fraction 0 and n, respectively, and Φ_{TS} and Φ_R are fractionation factors for exchangeable hydrogen sites in the transition and reactant states, respectively (*30*).

^{13}C KIE Studies of the wt ACCD-Catalyzed Reaction. ^{13}C kinetic isotope effects on k_{cat}/K_m for the wt ACCD-catalyzed reaction were measured by a competition experiment using the methodology developed by Singleton (*31*), wherein the ^{13}C enrichemnt at each carbon atom of the substrate (R/R_O) is measured by ^{13}C NMR spectroscopy and is used along with the fractional conversion of reactants (F) to calculate the $^{13}(k_{cat}/K_m)$ at each carbon atom via eq 6 (*31*−*35*)

$$KIE_{calc} = \ln(1 - F)/\ln[(1 - F)R/R_O] \quad (6)$$

For our purposes, R_O is the relative enrichment of ^{13}C (defined relative to the carboxyl carbon of ACC) at a specific carbon atom of an ACC sample prior to the reaction, R is the relative enrichment of ^{13}C at the same carbon atom in residual ACC recovered from a large-scale ACCD reaction mixture, and F is the fraction of reaction. Detailed descriptions of the large-scale reaction mixtures, purification protocols for residual ACC, ^{13}C NMR spectroscopy conditions, and the measurement of the fraction of reaction are all given in the Supporting Information,

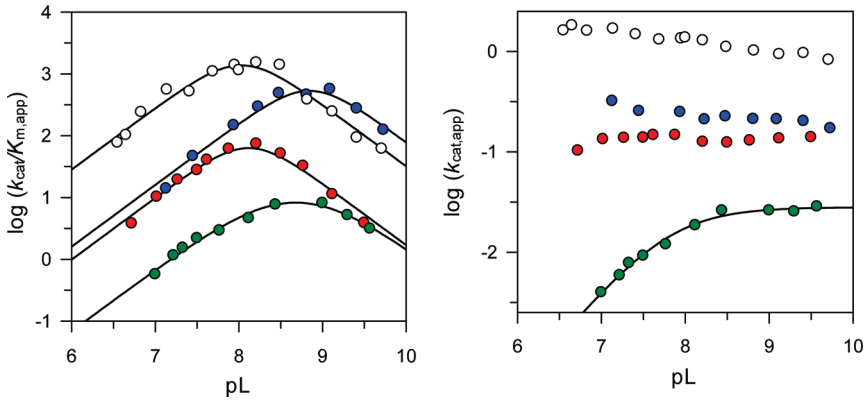

FIGURE 2: pH dependence of the steady state kinetic parameters for wt ACCD and its mutants (pL = pH or pD, pD = pH meter reading + 0.4): (white) wt ACCD in H_2O, (blue) wt ACCD in D_2O, (red) E295D in H_2O, and (green) Y268F in H_2O. The values of k_{cat} and K_m at each pH for each enzyme were determined by nonlinear regression of the initial velocity data using the Michaelis−Menten equation and are listed in Table S1 of the Supporting Information.

Table 1: Summary of the pH Dependence of the Steady State Kinetic Parameters for wt ACCD and Its Mutants[a]

enzyme	equation	k_{cat}/K_m (M^{-1} s^{-1})	pK_1	pK_2	pK'	k_{cat} (s^{-1})	pK_3	MSR
wt (H_2O)	1	$1.5(7) \times 10^4$	7.3(2)	8.7(2)	−	1.32(8)[b]	−	0.0134
wt (D_2O)	1	$9(5) \times 10^3$	7.9(3)	9.8(3)	−	0.22(2)[b]	−	0.0112
E295D	1	$2(1) \times 10^3$	6.9(2)	9.3(2)	−	0.132(4)[b]	−	0.0076
Y268F	2	$3.3(2) \times 10$	−	−	8.7(3)	−	−	0.0029
	3	−	−	−	−	0.028(1)	7.79(3)	0.0011

[a]See Materials and Methods for definitions of eqs 1−3. The standard errors in the last digit of each parameter estimate were obtained from the nonlinear fits to eqs 1−3 and are given in parentheses. MSR is the mean-square residual of the nonlinear fit. [b]Determined by averaging the k_{cat} values at each pH.

along with descriptions for calculating the standard error associated with the KIE measurement (*31*).

Stopped-Flow Absorption Measurements. Pre-steady state absorbance changes in the PLP chromophore were measured with a HI-TECH Scientific SF-61 double-mixing stopped-flow system equipped with a diode array detector for monitoring time-dependent changes in the PLP spectrum. The pH of all stock solutions was adjusted to the appropriate value immediately prior to conducting the experiments at 25 °C. The ionic strength of the final reaction mixtures was 150 mM. All concentrations given below correspond to those after mixing in the stopped flow. For wt ACCD, the reaction mixtures contained 100 μM enzyme and 50 mM ACC in 100 mM EPPS (pH 7.5). For Y268F, the reaction mixtures contained 96.5 μM enzyme and 50 mM ACC in 100 mM TAPS (pH 8.8). For E295D, the reaction mixtures contained 60 μM enzyme and 50 mM ACC and the reactions were performed in 100 mM MOPS (pH 7.5). For Y294F, the reaction mixtures contained 50 μM enzyme and 50 mM ACC and the reactions were performed in 100 mM MOPS (pH 7.5). The pre-steady state kinetic data were fit with exponential equations (of the form shown by eq 7) to estimate the amplitudes and rates associated with each observable kinetic phase

$$A_t = \sum_{1}^{n}[A_n(1 - e^{-k_n t})] + C \quad (7)$$

where A_t is the absorbance at a particular wavelength at time t after mixing, A_n and k_n are the observed amplitude and first-order rate constant, respectively, of kinetic phase n, and C is an offset that accounts for the absorbance at time zero.

RESULTS

Steady State Kinetic Studies. The pH dependence of the steady state kinetic parameters (k_{cat} and k_{cat}/K_m) was determined for wt ACCD, E295D, and Y268F over the pH range of 6.5−9.8 (Figure 2 and Table S1 of the Supporting Information). The initial velocity data were fit with eqs 1−3 to extract estimates for the apparent pK_a values of groups that contribute to substrate binding and catalysis, and estimates for the pH-independent values of the kinetic constants (Table 1). The k_{cat}/K_m profiles for each enzyme were fit with both eqs 1 and 2, and the fit that gave the lowest mean-square residual is reported. For wt ACCD and for E295D in H_2O, the fits to eq 1 give similar values for pK_1 (6.9−7.3) and pK_2 (8.7−9.3) as well as similar pH optima (8.0 and 8.1 for wt ACCD and E295D, respectively). For the wt ACCD reaction in D_2O, the apparent pK_1 and pK_2 values in the k_{cat}/K_m profile are both shifted to more basic pL, an expected result in 100% D_2O (*30*). For Y268F, the best fits were obtained with eq 2, which contains only a single apparent dissociation constant (pK' = 8.7). This pK' parameter is the average of two closely spaced apparent pK_a values. The relatively large errors associated with the k_{cat}/K_m parameter in each of the fits are likely due to the close separation of the apparent pK_a values governing the shape of the profiles.

Inspection of the k_{cat}−pH profiles reveals that this parameter is relatively independent of pH in the wt and E295D enzymes across the pH range tested. This indicates that if acid/base catalysis is involved in the rate-limiting step, the catalytic acid/base functional groups are not accessible to protonation and deprotonation in the enzyme−substrate/intermediate complexes. The k_{cat} parameter for E295D is reduced roughly 10-fold relative to that of wt ACCD across the pH range studied, and this accounts for the majority of the reduction in catalytic efficiency for the E295D mutant. Similar modest reductions in k_{cat} and k_{cat}/K_m have been observed in other PLP-dependent enzymes when the conserved Glu and Asp residues that interact with the pyridine N atom of the coenzyme are interchanged (*36*−*39*).

Scheme 4: Common Protonation States and Tautomeric Forms of Internal Schiff Bases

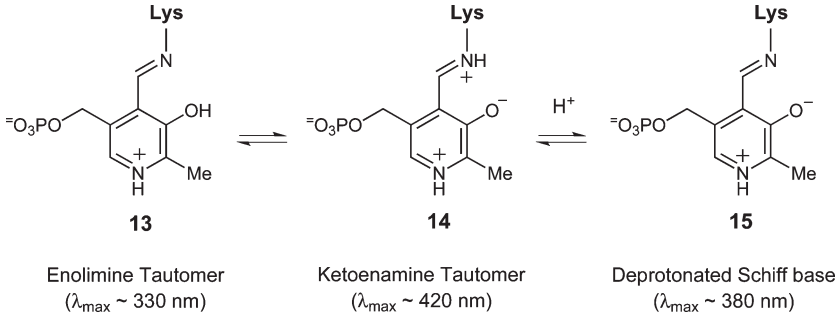

These data suggest an important catalytic function for Glu295. In contrast to those of wt ACCD and E295D, k_{cat} increases at high pH for the Y268F mutant, and fits of the data to eq 3 suggest that an active site group with a pK_a of ~7.8 needs to be deprotonated for catalysis. In this mutant, k_{cat} does not appear to level off at lower pH, suggesting that while there may be two forms of the Y268F−ACC Michaelis complex (one protonated and one unprotonated), only the unprotonated enzyme form is active. These results, along with the ~50-fold decrease in k_{cat} for the Y268F mutant, suggest that Tyr268 also plays an important role in catalysis.

pH Dependence of Internal Aldimine Absorption. The pH dependence of the electronic absorption of the internal aldimine was studied for the wt ACCD, Y268F, Y294F, and E295D enzymes. Protonated internal aldimines typically exhibit absorption bands near 330 and 420 nm, which correspond to the enolimine (**13**) and ketoenamine (**14**) tautomers of the protonated Schiff base (Scheme 4) (*40*). In contrast, deprotonated Schiff bases (**15**) typically exhibit an absorption maximum near 380 nm (*41*, *42*). In the resting state of each enzyme, absorption maxima are observed near 330 and 420 nm, consistent with the presence of both enolimine (**13**) and ketoenamine (**14**) forms of the internal aldimine (Figure 3 and Figure S1 of the Supporting Information), which coexist in many PLP enzymes at physiological pH (*38*, *43*−*48*). As the pH is increased, the ketoenamine tautomer (**14**) is converted to the enolimine tautomer (**13**). Importantly, there is no red shift in the λ_{max} of the ~330 nm peak at high pH in any of the enzymes, suggesting that the internal aldimine is not deprotonated (to **15**) as the pH is increased. Thus, the internal aldimine of ACCD and its mutants is likely protonated in the free enzyme form across the pH range assayed in this study. Correspondingly, the pK_1, pK_2, and pK_3 values determined from the kinetic−pH profiles likely correspond to other groups: either to active site amino acid side chains or to ionizable groups on the substrate. The pH dependence of the internal aldimine absorption may result from an enzyme conformational change that serves to alter the distribution between the ketoenamine and enolimine tautomers, but further investigation will be required to substantiate this claim.

Effects of Solvent Kinetic Isotopes and Viscosity on the wt ACCD-Catalyzed Reaction. To assess the involvement of solvent exchangeable protons in the reaction catalyzed by wt ACCD, we performed solvent KIE and viscosity variation studies with the wt enzyme. From the kinetic data reported in Table 1, significant solvent kinetic isotope effects [$^{D_2O}k_{cat} = k_{cat,H_2O}/k_{cat,D_2O} = 5.7$, and $^{D_2O}k_{cat}/K_m = (k_{cat}/K_m)_{H_2O}/(k_{cat}/K_m)_{D_2O} = 2.5$] were calculated for the wt enzyme using the data collected at the pL optimum in each solvent (8.1 in H_2O and 8.8 in D_2O). This result clearly suggests that solvent exchangeable protons play an important role in ACCD catalysis, and that bonds involving solvent exchangeable protons are likely breaking in the step(s) that limit steady state turnover. The larger magnitude of $^{D_2O}k_{cat}$ relative to $^{D_2O}k_{cat}/K_m$ suggests that there may be solvent kinetic isotope effects on steps following the first irreversible step in the mechanism, which is assumed to be the ACC cyclopropane ring cleavage step. Inspection of both of the putative mechanisms for ACCD catalysis (Schemes 2 and 3) shows that there are several possible steps following the $C_\alpha-C_\beta$ bond cleavage that could potentially exhibit solvent KIEs.

Because the relative viscosity of 100% D_2O solutions is higher than that of 100% H_2O solutions (*49*), it is possible that the apparent solvent KIEs may actually be due to the variation in solvent viscosity when H_2O is replaced with D_2O. It is known that increasing the solvent viscosity can lower the diffusion coefficient of solutes which, in turn, can slow the rates of bimolecular association and dissociation processes (*50*−*52*). In the case of enzyme catalysis, viscosity effects are often manifested on steps in the kinetic mechanism involving substrate−product binding or release, or when large-scale unimolecular enzyme conformational changes occur (*52*−*58*). To assess the dependence of the wt ACCD-catalyzed reaction on solvent viscosity, the effect of glycerol concentration on the reaction rate under pseudo-first-order conditions was analyzed (Figure S2 of the Supporting Information). Fitting the kinetic data to eq 4 gives a slope that is not significantly different than zero ($S = 0.05 \pm 0.05$), demonstrating that k_{cat} is not limited by product dissociation or large-scale enzyme conformational changes under these conditions. These results indicate that the $^{D_2O}k_{cat}$ is a legitimate solvent KIE and is not the result of increasing the relative viscosity of the solvent.

Proton Inventory for the wt ACCD-Catalyzed Reaction. A proton inventory study was conducted to further explore the large solvent KIE measured on k_{cat} for the wt ACCD reaction (*30*). The k_{cat} versus pL profiles for the wt ACCD reaction indicated that k_{cat} is relatively independent of pL over the entire pL range assayed (Figure 2). Hence, we chose to perform the proton inventory studies at pL 8.0 with 30 mM ACC, which is well above the K_m for ACC in both 100% H_2O and 100% D_2O at pL 8.0 (see Table S1 of the Supporting Information). The nonlinear fits of the proton inventory data to several different forms of eq 5 are shown in Figure 4 along with the residual plots. The definitions of the various forms of eq 5 used to fit the data and a summary of the fitted parameters are listed in Table 2. The best fits, as evidenced by the residual plots (Figure 4) and lack of fit F tests (Table S2 of the Supporting Information), were obtained with models where multiple transition state protons are moving in the step(s) that limit turnover under pseudo-first-order conditions (the T_2 and T_1S models). The simple linear

model (T_1) did not exhibit any significant lack of fit at the 95% confidence interval (Table S2 of the Supporting Information). However, from the residual plot for the fit to this model (Figure 4), there appear to be systematic deviations between the fitted curve and the mean value of the data points. Because of this, the T_2 and T_1S models appear to be more appropriate models for fitting the proton inventory data.

The slightly bowl-shaped curvature of the proton inventory plots suggests that $^{D_2O}k_{cat}$ is composed of at least two, normal solvent KIEs (*30*). In both the T_2 and T_1S models, one exchangeable site (Φ_1) is predicted to be responsible for the majority of the solvent KIE on k_{cat} (Φ_1 = 0.3−0.33; KIE = 3.0−3.3), while a second site (Φ_2) or set of sites (Φ_S) contributes a smaller normal effect (KIE ∼ 1.4−1.5). On the basis of the measured differences in $^{D_2O}k_{cat}$ (5.7) and $^{D_2O}k_{cat}/K_m$ (2.5) discussed above, our hypothesis is that one of the two normal solvent KIEs is expressed on a step prior to or concomitant with cyclopropane ring cleavage (thus contributing to both $^{D_2O}k_{cat}$ and $^{D_2O}k_{cat}/K_m$), while the other normal solvent KIE is expressed on a step (or steps) following cyclopropane ring cleavage (and is expressed only on k_{cat}).

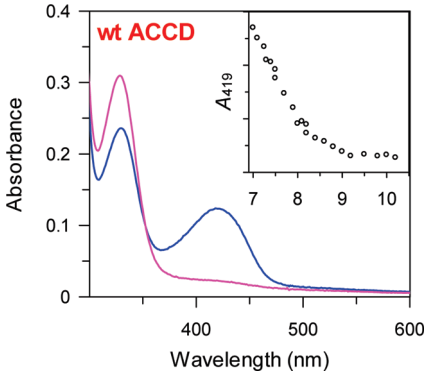

FIGURE 3: UV−visible absorption spectra of the low-pH (blue spectra) and high-pH (fuscia spectra) forms of the internal aldimine (**3**) of wt ACCD. The pH dependence of the absorption at 419 nm is shown in the inset to the panel. Similar pH-dependent absorption changes were also seen with the E295D, Y268F, and Y294F mutant enzymes (see Figure S1 of the Supporting Information).

^{13}C Kinetic Isotope Effects. To determine if the step in the ACCD-catalyzed reaction involving the cleavage of the cyclopropane ring of ACC contributes to steady state rate limitation under k_{cat}/K_m conditions, a ^{13}C KIE study of the wt ACCD-catalyzed reaction was conducted using the method developed by Singleton, which allows for the simultaneous determination of $^{13}(k_{cat}/K_m)$ at each carbon atom of the substrate (*31*). As the wt ACCD-catalyzed reaction approaches completion, any residual ACC starting material in the reaction mixture will be enriched in ^{13}C at the C_α and *pro-S* C_β positions if there is a ^{13}C KIE on k_{cat}/K_m. This is because ACC molecules containing ^{13}C at the scissile *pro-S* C_β−C_α bond will react more slowly than ACC molecules containing ^{12}C at the scissile bond. The relative ^{13}C enrichment of unreacted and residual samples of ACC (R_O and R, respectively) is measured by ^{13}C NMR spectroscopy and is used to calculate the enrichment ratio (R/R_O). This value is then used, along with the fraction of reaction (F), to calculate the KIE at each carbon atom via eq 6 (*35*).

A typical ^{13}C NMR spectrum for ACC acquired under the NMR conditions reported in the Supporting Information is shown in Figure S3. The ^{13}C peak integrations from each of the replicate NMR spectra of each ACC sample and the replicate measurements of the fraction of reaction are listed in Tables S3 and S4 of the Supporting Information, respectively. The R/R_O and F observables and their standard errors calculated from these data for each of the two replicate large-scale reactions are listed in Table 3, along with the calculated KIEs on C_α and *pro-S* C_β. Equation 6 was used to calculate the KIE at C_α. However, the ^{13}C NMR signals for the *pro-R* and *pro-S* β-carbons of ACC are

Table 2: Summary of Fits of the Proton Inventory Data to Various Forms of the Gross−Butler Equation (eq 5)

model	equation (k_n/k_o =)	k_o	Φ_1	Φ_2	Φ_S	MSR
T_1	$1 - n + n\Phi_1$	0.60(1)	0.19(1)	–	–	0.00043
T_2	$(1 - n + n\Phi_1)(1 - n + n\Phi_2)$	0.61(1)	0.33(7)	0.7(1)	–	0.00024
T_1S	$(1 - n + n\Phi_1)\Phi_S{}^n$	0.61(1)	0.30(4)	–	0.7(1)	0.00023

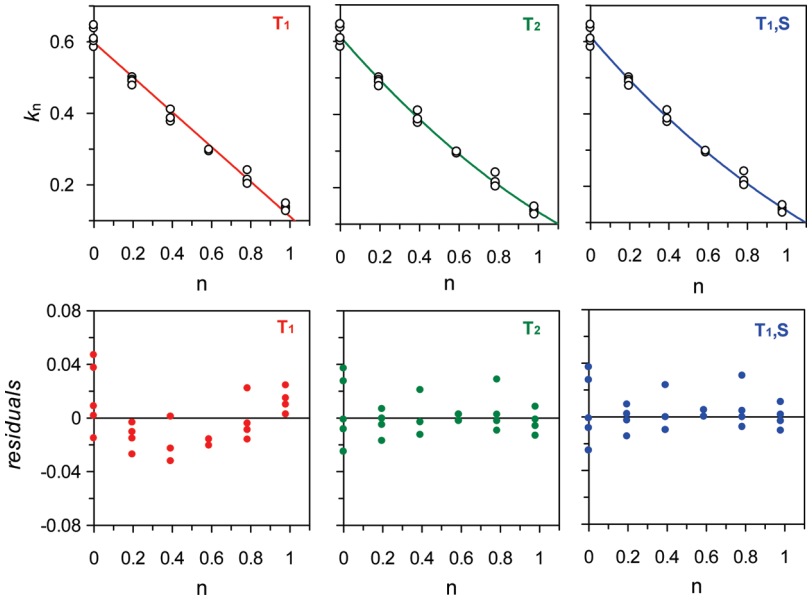

FIGURE 4: Proton inventory data for wt ACCD. See Table 2 for the definition of each model (T_1, T_2, and T_1S) and for the values of the fitted parameters.

Table 3: Summary of $^{13}k_{cat}/K_m$ Data for the wt ACCD Reaction[a]

reaction	$R/R_{O(C\alpha)}$	$\Delta R/R_{O(C\alpha)}$	$R/R_{O(C\beta)}$	$\Delta R/R_{O(C\beta)}$	F	ΔF	$^{13}(k_{cat}/K_m)_{C\alpha}$	$^{13}(k_{cat}/K_m)_{C\beta}$
1	1.031	0.017	1.000[b]	0.005	0.906	0.006	1.013(7)	1.000(5)[b]
2	1.030	0.010	1.031	0.006	0.834	0.006	1.017(6)	1.034(3)
average							1.015(5)	1.017(17)

[a] R/R_O and its standard error ($\Delta R/R_O$) were calculated from the NMR data in Table S3 of the Supporting Information. F and its standard error (ΔF) were calculated from the LDH reporter assay data in Table S4 of the Supporting Information. $^{13}(k_{cat}/K_m)_{C\alpha}$ and $^{13}(k_{cat}/K_m)_{C\beta}$ were then calculated from R/R_O and F using eqs 6 and 8, respectively, and the standard errors in the final digit of the KIE measurements (in parentheses) were calculated using eqs S2−S4 of the Supporting Information. The arithmetic average (and its standard error) of the two replicate measurements for each ^{13}C KIE was then calculated to determine the reported KIE. [b] The R/R_O of unity yields no error in eqs S2 and S3 of the Supporting Information. For calculation of the average value of $^{13}(k_{cat}/K_m)_{C\beta}$, we assumed a relative error of 0.5% on $^{13}(k_{cat}/K_m)_{C\beta}$ for reaction 1 (the average relative error of the other KIE measurements).

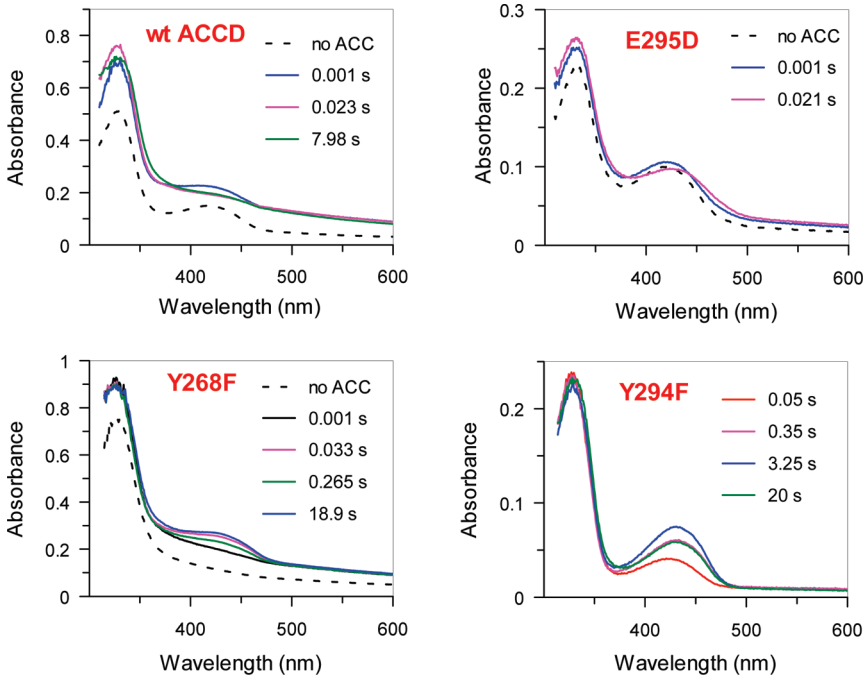

FIGURE 5: Multiwavelength stopped-flow studies of wt ACCD and its mutants. The times in each panel indicate the time after mixing with 50 mM ACC. For each enzyme, time-dependent absorption changes in the ~430 nm region were also fit with the appropriate exponential expression (eq 8) to extract estimates for rates and amplitudes of each observable kinetic phase (see Figure S4 and Table S6 of the Supporting Information).

indistinguishable, yielding an observed, combined enrichment ($R^\beta = R^{pro\text{-}S} + R^{pro\text{-}R}$) versus the reference. If the initial enrichment at each β-carbon is the same, then the values of $R^{pro\text{-}S}$ and $R^{pro\text{-}R}$ prior to reaction are both given by the equation $R_O{}^{pro\text{-}S} = R_O{}^{pro\text{-}R} = R_O{}^\beta/2$, where $R_O{}^\beta$ is the observed, combined enrichment prior to reaction. Next, if we assume that only the *pro-S* β-carbon exhibits a nonunit isotope effect, then the observed, combined enrichment at some fraction of reaction F will be given by the equation $R^\beta = R^{pro\text{-}S} + R_O{}^{pro\text{-}R}$ (or $R^\beta = R^{pro\text{-}S} + R_O{}^\beta/2$) because $R^{pro\text{-}R}$ remains equal to its initial value. Therefore, the ratio of interest for computing the isotope effect associated with the *pro-S* β-carbon alone, i.e., $R^{pro\text{-}S}/R_O{}^{pro\text{-}S}$, can be calculated as $2R^\beta/R_O{}^\beta - 1$:

$$KIE_\beta = \ln(1-F)/\ln[(1-F)(2R^\beta/R_O{}^\beta - 1)] \qquad (8)$$

The calculated $^{13}(k_{cat}/K_m)$ values on the C_α and *pro-S* C_β atoms of ACC from the two replicate measurements were then averaged together to give ^{13}C KIEs of 1.015 ± 0.005 on C_α and of 1.017 ± 0.017 on *pro-S* C_β. Unfortunately, while $^{13}(k_{cat}/K_m)_\alpha$ appeared to be significantly larger than unity in both reactions, the average $^{13}(k_{cat}/K_m)_\beta$ was within error of unity. Nevertheless, the 1.5% isotope effect at C_α (Table 3) compares favorably with $^{13}k_{cat}/K_m$ isotope effects measured for other enzyme-catalyzed reactions (*59*−*64*) and suggests that the C_α−C_β bond cleavage step in ACCD catalysis is at least partially rate-limiting under k_{cat}/K_m conditions.

Multiwavelength Stopped-Flow Studies. In an attempt to identify and characterize the PLP-linked intermediates that form during turnover under saturating ACC concentrations, absorption spectra for wt ACCD and its E295D, Y268F, and Y294F mutants were collected with a stopped-flow apparatus using a diode array detector (Figure 5). In the fast reaction phase for the wt enzyme, the ketoenamine tautomer of the internal aldimine (λ_{max} = 419 nm) is converted into a new species (λ_{max} = 329 nm) with an apparent rate constant k_1 of 260 s^{-1} (Figure S4 and Table S5 of the Supporting Information). This species is most likely either the enolimine form of an external aldimine or the *gem*-diamine species that is observed in the crystal structure (*21*) and that also has an absorption maximum in the 330 nm region (*65*). Following the fast phase, there is a slower phase occurring at a catalytically competent observed rate [k_2 = 2.3 s^{-1} (Figure S4 of the Supporting Information)], during which the 329 nm absorption band decreases in intensity and is broadened slightly.

In contrast to that of the wt enzyme, the λ_{max} values of both of the internal aldimine peaks (λ_{max} = 331 and 421 nm) in the E295D mutant shift slightly upon mixing with ACC to values of 329 and

~428 nm, respectively, at an observed first-order rate constant k_1 of ~150 s^{-1} (Figure S4 of the Supporting Information). The spectral shifts are associated with a slight decrease in the absorption intensity in the ~420 nm region and a corresponding increase in the ~330 nm region. Similar rapid spectral shifts have been observed in other PLP-dependent enzymes and are usually attributed to the formation of an external aldimine intermediate, whose absorption properties often differ slightly from those of the internal aldimine (*66*). In the Y268F mutant, a species with a λ_{max} at 431 nm forms upon mixing with ACC at an observed rate k_1 of 70 s^{-1}. As in the E295D mutant, the λ_{max} of this intermediate is red-shifted relative to the λ_{max} of the ketoenamine tautomer of the internal aldimine [419 nm (see Figure S1 of the Supporting Information)], suggesting that the external aldimine is likely accumulating upon binding of ACC to Y268F. The absorbance changes at 431 nm are triphasic, and interestingly, the intensity of the 431 nm absorption band increases during the fast phase ($k_1 \sim 70$ s^{-1}), decreases over the next ~200 ms ($k_2 \sim 15$ s^{-1}), and then increases again over the next several seconds in a slow phase [$k_3 \sim 0.5$ s^{-1} (Figure S4 of the Supporting Information)]. All three kinetic phases are fast enough to be kinetically competent (see Tables S1 and S6 of the Supporting Information). In the catalytically inactive Y294F mutant (*20*), the ketoenamine form of an external aldimine (λ_{max} = 431 nm) also appears to accumulate upon ACC binding. Support for this assignment is provided by the crystal structure of the yeast Y295F enzyme (analogous to the *Pseudomonas* sp. ACP Y294F mutant) determined in the presence of ACC, where an external aldimine species was detected (*19*). Like the Y268F reaction, the absorbance changes in the Y294F mutant at 431 nm upon ACC binding were multiphasic. However, in the case of Y294F, the 431 nm absorption increased in the fast phase (k_1 = 6.1 s^{-1}) and then continued to increase in an intermediate phase (k_2 = 0.5 s^{-1}) before decaying in a slow phase [k_3 = 0.1 s^{-1} (Figure S4 of the Supporting Information)].

DISCUSSION

On the basis of the kinetic characterization of wt ACCD and its mutants reported in this study, a working model for the pH dependence of the steady state kinetic parameters and the protonation states of the important active site residues can be proposed (Scheme 5). The group responsible for pK_1 is assigned to the phenoxyl group or Tyr294, which likely needs to be deprotonated for ACC binding. Support for this conclusion is derived from the similarity of pK_1 in the wt and E295D mutant enzymes and from the increase in pK_1 of ~1.5 units in the Y268F enzyme. In this model, the pK_a of Tyr294 is lowered by its hydrogen bonding interaction with Tyr268 [2.5 Å (Figure 1)], which allows ACC to bind and Tyr294 to deprotonate the amino group of ACC, facilitating the aldimine exchange reaction. A role for Tyr294 in ACC deprotonation was first proposed on the basis of structural studies by Ose et al. (*19*) and is also supported by our stopped-flow studies of the Y294F mutant, in which the rate of the aldimine exchange reaction to form an external aldimine is significantly reduced.

The pK_2 values determined from the k_{cat}/K_m−pH profiles are relatively invariant, suggesting that this apparent ionization constant likely corresponds either to the amino group of ACC or to the side chain of Ser78. The pK_a of cyclopropylamine is ~8.7 in aqueous solution (*67*), which is very similar to the kinetic pK_2 values (~9) measured in our studies. A protonated, positively charged ACC amino group could engage in favorable electrostatic interactions with the deprotonated, negatively charged Tyr294 to facilitate ACC binding. Alternatively, if Ser78 is responsible for pK_2, Ser78 would likely need to be protonated to form a hydrogen bond to the ACC carboxylate group (see Figure 1). The pK_a of the hydroxyl side chain of Ser78 may be lowered by hydrogen bonding interactions with the backbone amide groups of Gln80 and Thr81 and/or through a putative helix−dipole interaction. Similar helix−-dipole interactions have been shown to lower the pK_a of Cys residues in model peptides (*68*) and in enzyme active sites (*69*, *70*) by nearly two units. The lowering of the pK_a of Ser78 could also serve a catalytic function, as this residue has been implicated in acid/base chemistry during turnover, perhaps serving to mediate proton transfers at C3 of the substrate−PLP adduct following cyclopropane ring scission (*22*). Finally, spectroscopic studies of the internal aldimines of wt ACCD, Y268F, Y294F, and E295D demonstrate that the Schiff base remains protonated across the pH range studied, suggesting that the deprotonation of PLP is not responsible for pK_2.

Analysis of the kinetic properties of the ACCD mutant enzymes provides insight into the chemical mechanism for cyclopropane ring cleavage. PLP species consistent with the ketoenamine tautomer of an external aldimine (**4**, Scheme 5) form in the pre-steady state fast phases of the E295D- and Y268F-catalyzed reactions. Because the external aldimine is an essential intermediate in nucleophile-induced ring scission but is not required in acid-catalyzed ring cleavage, the detection of **4** suggests that the acid-catalyzed strategy shown in Scheme 3 is probably not employed in the mutant enzymes. Stronger evidence of a nucleophile-induced ring scission is provided by the k_{cat}−pH profile for the Y268F mutant, where an active site group in the Michaelis complex with a pK_a of ~7.8 must be deprotonated for activity. The most likely candidate for this important catalytic group is the side chain of Tyr294. This conclusion is supported by the conservation of the Tyr268-Tyr294 pair in ACCD homologues, the close proximity of the phenoxyl groups of Tyr294 and Tyr268 (2.5 Å), the position of the Tyr294 phenoxyl group near the *pro-S* C_β of ACC in the cocrystal structure (3.0 Å), and the complete inactivity of the Y294F mutant (*18*, *19*, *21*). The 10-fold reduction in k_{cat} for the E295D mutant and the reported inactivity of the E295Q mutant (*19*) are also most consistent with the nucleophile-induced ring cleavage mechanism. The weakened ion pair interaction between the carboxylate group of Glu295 and the pyridinium nitrogen of PLP in the E295D mutant may increase the energy of the transition state for the ring scission step if the liberated cyclopropane ring electrons cannot be delocalized efficiently into the coenzyme.

Interestingly, a clearly definable ketoenamine tautomer of an external aldimine species cannot be detected in the presteady state of the wt ACCD reaction. Instead, a species consistent with either an enolimine tautomer of an internal/external aldimine or a *gem*-diamine (**10**, Scheme 5) accumulates rapidly at an observed rate constant of ~260 s^{-1} at saturating ACC concentrations. Although the observed PLP intermediate is spectroscopically indistinguishable from the enolimine tautomer of the internal aldimine resting state, the attack of the incoming ACC amino group on the C4′ atom of PLP to initiate the aldimine exchange is expected to be fast in the wt enzyme, in light of the observations that the Y268F and E295D mutant enzymes quickly catalyze the aldimine exchange reaction. Thus, the observable species in the stopped-flow studies of the wt enzyme is tentatively assigned as the *gem*-diamine that is

Scheme 5: Revised Chemical Mechanism for ACCD[a]

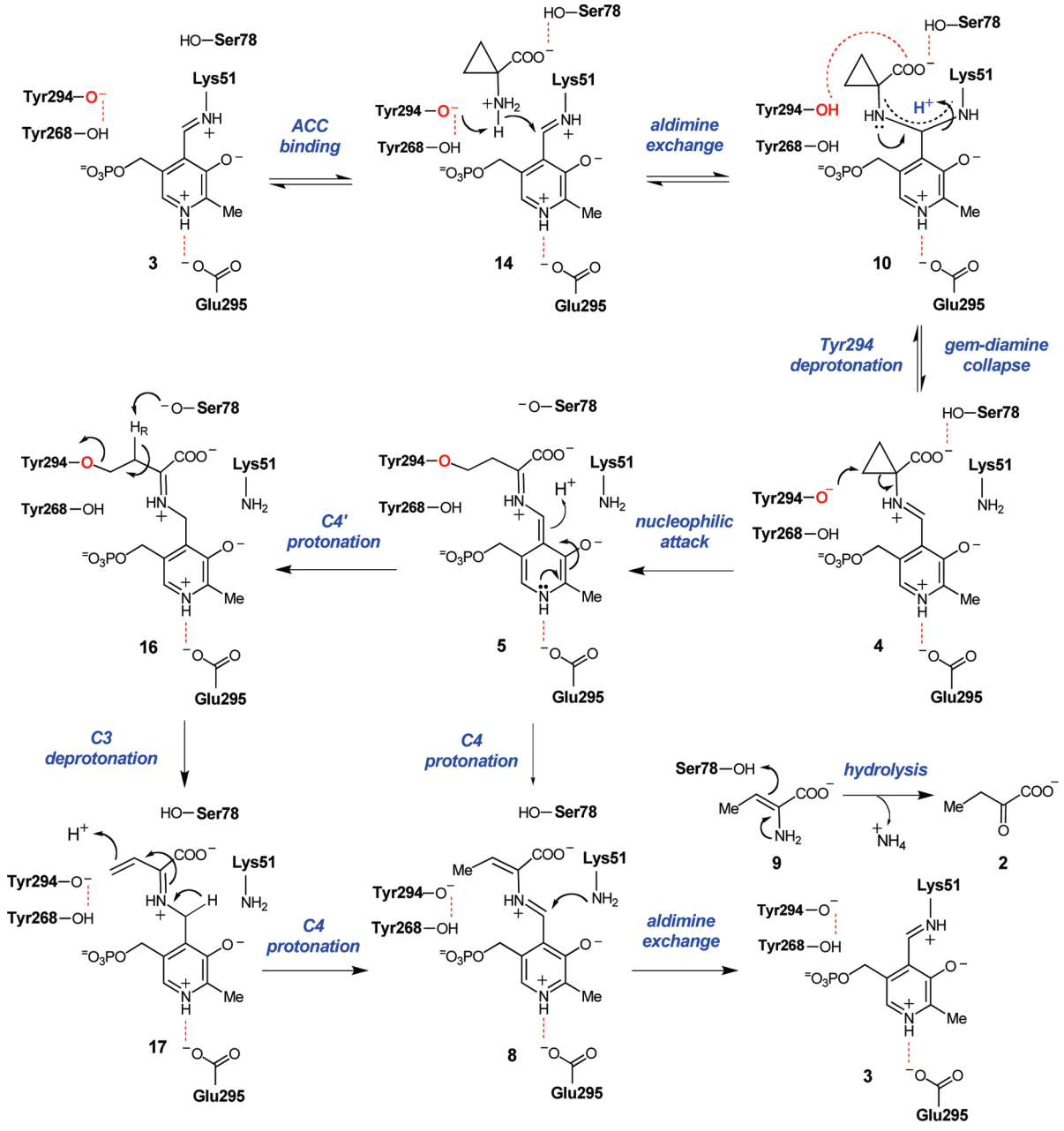

[a]Putative hydrogen bonds are shown as dashed lines.

observed in the X-ray crystal structure of the wt ACCD enzyme in the presence of ACC (*20*, *21*).

According to our model for substrate binding and catalysis (Scheme 5), the side chain of Tyr294 is protonated in the *gem*-diamine state of the wt ACCD−ACC complex, allowing it to form a hydrogen bond with the ACC carboxylate group (2.7 Å). It is possible that deprotonation of Tyr294 in the Michaelis complex and the collapse of the *gem*-diamine into the external aldimine (**10** → **4**) are energetically demanding, allowing the *gem*-diamine species to accumulate in the presteady state. A similar *gem*-diamine intermediate also accumulates in incubations of wt ACCD with 1-aminocyclopropane 1-phosphonate (ACP) which, despite its stereoelectronic properties being similar to those of ACC, is not turned over into any products (*21*, *65*). Interestingly, the internuclear distance between the oxygen atom of the Tyr294 side chain and the phosphonate oxygen of ACP in the *gem*-diamine form of the ACP−ACCD complex (2.3 Å) is shortened relative to the distance between Tyr294 and the ACC carboxylate group in the *gem*-diamine form of the ACC−ACCD complex (2.7 Å) (*21*). It is tempting to speculate that this shortened hydrogen bond distance could help to trap the ACP−ACCD complex in an unreactive *gem*-diamine state, perhaps accounting for the slow, tight binding inhibition properties of ACP (*65*). At present, it is still unclear why the aldimine exchange reaction in wt ACCD is halted in the *gem*-diamine state while both the Y268F and E295D mutants can apparently move quickly through this intermediate to generate the external aldimine rapidly in the presteady state. On the basis of this unusual observation and the fact that the ACP inhibitor also forms a *gem*-diamine complex when bound to wt ACCD, it is possible that the *gem*-diamine species detected in the wt ACCD-catalyzed reaction is an off-pathway species.

Scheme 6: Putative Mechanism for ACCD Catalysis Involving Concerted Deprotonation and Nucleophilic Addition

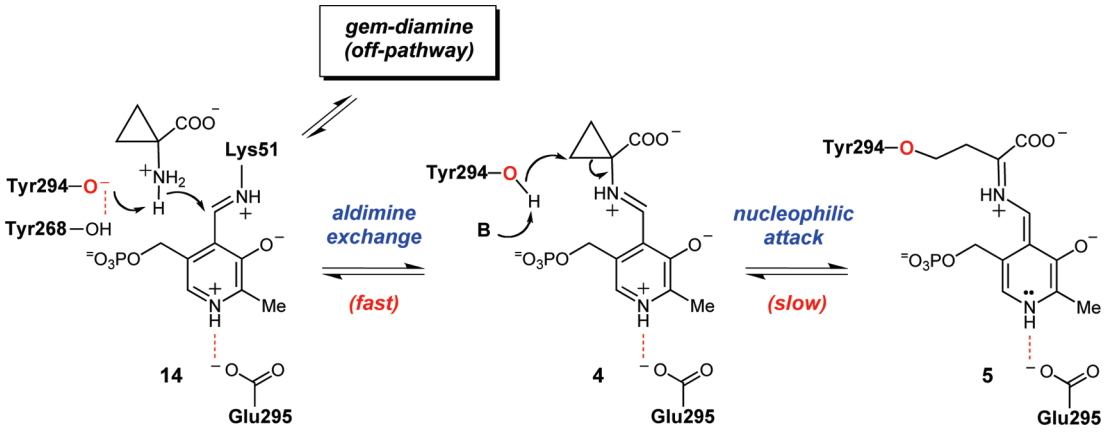

The proposed mechanism for ACCD catalysis involving nucleophilic addition of Tyr294 to the cyclopropane ring of ACC (Scheme 5) can be rationalized on the basis of the solvent and ^{13}C kinetic isotope effects determined in this study. The interpretation of the KIEs depends on whether the putative *gem*-diamine species (**10**) is a catalytically competent intermediate. If **10** is a species on the reaction pathway, the steps leading from *gem*-diamine decay to the external aldimine (**10** → **4**) and from the external aldimine to the quinonoid species (**4** → **5**) may both be partially rate-limiting during steady state turnover under k_{cat}/K_m conditions. Here, the normal $^{D_2O}k_{cat}/K_m$ of 2.5 could be a result of the decay of the *gem*-diamine species. Deprotonation of Tyr294 and/or protonation of the amino side chain of Lys51 during its elimination from the *gem*-diamine intermediate could potentially generate the normal solvent KIE on k_{cat}/K_m. The $^{13}(k_{cat}/K_m)$ isotope effect of 1.5% on C_α of ACC would arise from the partially rate-limiting conversion of the reactive external aldimine intermediate to the quinonoid (**4** → **5**). The magnitude of $^{13}(k_{cat}/K_m)$ on the wt ACCD-catalyzed reaction is modest when compared to the ~4−6% KIEs measured for enzymatic PLP-dependent decarboxylation reactions when the decarboxylation step is fully rate-limiting (*62*, *63*). The modest $^{13}(k_{cat}/K_m)$ on the wt ACCD-catalyzed reaction would be consistent with a stepwise mechanism in which the ^{13}C KIE is attenuated by a preceding and partially rate limiting *gem*-diamine decay step.

Alternatively, if the *gem*-diamine species (**10**) that accumulates in the wt ACCD-catalyzed reaction is an off-pathway intermediate, the solvent and ^{13}C KIEs could be reporting on the same step in the mechanism. Here, the external aldimine would be generated rapidly upon ACC binding to the wt enzyme (Scheme 6) but may represent an only minor fraction of the total enzyme present in the reaction mixtures with ACC (with the major enzyme form being a nonproductive *gem*-diamine state). As such, the external aldimine could elude detection by stopped-flow absorption spectroscopy. In this concerted mechanism, Tyr294 deprotonation could occur concomitantly with nucleophilic attack and $C_\beta-C_\alpha$ bond cleavage. The magnitude of the solvent KIE for wt ACCD ($^{D_2O}k_{cat}/K_m$ = 2.5) is consistent with solvent KIE values measured for enzymatic reactions in which deprotonation of oxygen nucleophiles is concerted with nucleophilic attack (*71*). In this scenario, the 1.5% $^{13}(k_{cat}/K_m)$ on the ACCD-catalyzed reaction could indicate an early (or late) transition state for C−C bond cleavage, rather than a stepwise mechanism in which the C−C bond cleavage step is only partially rate-limiting. According to the Hammond Postulate, an early transition state for C−C bond cleavage would be expected for the exothermic cyclopropane ring opening event.

Following cleavage of the ACC cyclopropane ring, transient protonation at C4′ of PLP to form the ketimine species (**16**) may help to activate the C_β proton (at C3) by lowering the anionic character at C_α (Scheme 5), in analogy to the reaction catalyzed by cystathionine γ-synthase (*72*). The tyrosine nucleophile could then be eliminated from **16** by deprotonation of the *pro-R* proton at C3, yielding the β,γ-unsaturated ketimine intermediate (**17**). On the basis of stereochemical (*9*, *16*), structural (*18*−*21*), and biochemical studies (*22*), Ser78 is the most likely candidate for catalyzing this deprotonation. Most notably, the catalytic efficiency of the S78A mutant is significantly reduced; Ser78 is covalently modified by the electrophilic ACC analogue, 2-methylene-ACC, and Ser78 is required for C_α deprotonation of ACCD-bound D-amino acid−PLP adducts (*22*). Protonation at C_γ of the quinonoid species (**17**) to give the PLP−aminocrotonate species (**8**), followed by aldimine exchange (**8** → **3**), and hydrolysis of the aminocrotonate (**9** → **2**) would complete the catalytic cycle. The groups responsible for mediating these transformations are not clear, but they likely involve some level of participation by Tyr268, Tyr294, Ser78, Lys51, and the PLP. Because these steps follow the irreversible cyclopropane ring cleavage step, one or more of them is likely responsible for the additional portion of the normal solvent KIE that is measured on only k_{cat}. At this point, the irreversibility of the ACCD-catalyzed reaction and our inability to conclusively detect species **5**, **16**, **17**, and **8** in the wt ACCD reaction using stopped-flow spectroscopy have made characterization of the late stages of the reaction mechanism difficult.

Taken together, the accumulated evidence strongly favors a mechanism for ACCD catalysis involving nucleophilic cleavage of the cyclopropane ring. However, the unusual stability of the *gem*-diamine intermediate in the wt ACCD−ACC complex prompted us to propose an alternative mechanism (Scheme 3) in which Tyr294 acts as a general acid to facilitate the opening of the cyclopropane ring of ACC (*20*). Precedence for a similar mode of electrophilic cyclopropane ring cleavage has been provided by Jencks and co-workers in their model studies of the reactivity of phenylcyclopropanols (*23*). Though this mechanism cannot be rigorously excluded at the moment, it is at odds with several experimental observations. First, for the E295D and Y268F enzymes, an external aldimine intermediate accumulates in the presteady state, which is not predicted to form along the putative reaction coordinate for the acid-catalyzed ring opening

mechanism. Second, incorporation of a solvent proton into C_γ of the α-KB product is not fully stereospecific (*16*), which is unlikely if Tyr294 is serving as a general acid to initiate ring cleavage from the *gem*-diamine intermediate. Third, the E295Q mutant is inactive (*19*), and the activity of the E295D mutant is substantially decreased. These observations suggest that electron delocalization into the pyridinium ring (a hallmark of normal PLP catalysis that would not be required for turnover in the acid-catalyzed mechanism) is an important feature of wt ACCD catalysis. Finally, in addition to the deamination of ACC, wt ACCD catalyzes a variety of C_α deprotonation and C_β elimination reactions with other amino acid substrates (*9*, *11*, *22*). These reactions most likely proceed via quinonoid species that are common to many other PLP-dependent enzyme mechanisms. Thus, the wt ACCD enzyme is at least capable of accommodating these typical PLP intermediates, which would not be employed in the acid-catalyzed ring opening mechanism.

ACKNOWLEDGMENT

We thank Dr. Mark Ruszczycky and Professor Christian P. Whitman for their critical reading of the manuscript, Professor Paul Cook for his helpful discussions, Dr. Zhihua Tao for constructing some of the mutant enzymes employed in this study, and Steve Sorey for his assistance with the NMR experiments.

SUPPORTING INFORMATION AVAILABLE

Steady state kinetic data, error analysis for the proton inventory studies, raw data used for the calculation of the ^{13}C KIEs, and nonlinear fits of the stopped-flow data. This material is available free of charge via the Internet at http://pubs.acs.org.

REFERENCES

1. Honma, M., and Shimomura, T. (1978) Metabolism of 1-aminocyclopropane-1-carboxylic acid. *Agric. Biol. Chem. 42*, 1825–1831.
2. Kende, H. (1993) Ethylene biosynthesis. *Annu. Rev. Plant Physiol. Plant Mol. Biol. 44*, 283–307.
3. Klee, H. J., Hayford, M. B., Kretzmer, K. A., Barry, G. F., and Kishore, G. M. (1991) Control of ethylene synthesis by expression of a bacterial enzyme in transgenic tomato plants. *Plant Cell 3*, 1187–1193.
4. Eliot, A. C., and Kirsch, J. F. (2004) Pyridoxal phosphate enzymes: Mechanistic, structural, and evolutionary considerations. *Annu. Rev. Biochem. 73*, 383–415.
5. Dunathan, H. C. (1966) Conformation and reaction specificity in pyridoxal phosphate enzymes. *Proc. Natl. Acad. Sci. U.S.A. 55*, 712–716.
6. Toney, M. D. (2005) Reaction specificity in pyridoxal phosphate enzymes. *Arch. Biochem. Biophys. 433*, 279–287.
7. Matthews, R. B., and Drummond, J. T. (1990) Providing one-carbon units for biological methylations: Mechanistic studies on serine hydroxymethyltransferase, methylenetetrahydrofolate reductase, and methyltetrahydrofolate-homocysteine methyltransferase. *Chem. Rev. 90*, 1275–1290.
8. Schirch, V., and Szebenyi, D. M. E. (2005) Serine hydroxymethyltransferase revisited. *Curr. Opin. Chem. Biol. 9*, 482–487.
9. Walsh, C. T., Pascal, R. A., Jr., Johnston, M., Raines, R., Dikshit, D., Krantz, A., and Honma, M. (1981) Mechanistic studies on the pyridoxal phosphate enzyme 1-aminocyclopropane-1-carboxylate deaminse from *Pseudomonas* sp. *Biochemistry 20*, 7509–7519.
10. Hill, R. K., Prakash, S. R., Wiesendanger, R., Angst, W., Martinoni, B., Arigoni, D., Liu, H.-w., and Walsh, C. T. (1984) Stereochemistry of the enzymatic ring opening of 1-aminocyclopropanecarboxylic acid. *J. Am. Chem. Soc. 106*, 795–796.
11. Li, K., Du, W., Que, N. L. S., and Liu, H.-w. (1996) Mechanistic studies of 1-aminocyclopropane-1-carboxylate deaminase: Unique covalent catalysis by coenzyme B_6. *J. Am. Chem. Soc. 118*, 8763–8764.
12. Stewart, J. M., and Westberg, H. H. (1965) Nucleophilic ring-opening additions to 1,1-disubstituted cyclopropanes. *J. Org. Chem. 30*, 1951–1955.
13. Yates, P., Helferty, P. H., and Mahler, P. (1983) Nucleophilic and acid-catalyzed cleavage of the cyclopropane rings of β,γ-unsaturated α-spirocyclopropyl ketones. *Can. J. Chem. 61*, 71–85.
14. Danishefsky, S. (1979) Electrophilic cyclopropanes in organic synthesis. *Acc. Chem. Res. 12*, 66–72.
15. Cleland, W. W. (1982) The use of pH studies to determine chemical mechanisms of enzyme-catalyzed reactions. *Methods Enzymol. 87*, 390–405.
16. Liu, H.-w., Auchus, R., and Walsh, C. T. (1984) Stereochemical studies on the reactions catalyzed by the PLP-dependent enzyme 1-aminocyclopropane-1-carboxylate deaminase. *J. Am. Chem. Soc. 106*, 5335–5348.
17. Battiste, M. A., and Coxon, J. M. (1987) Acidity and basicity of cyclopropanes. In The chemistry of the cyclopropyl group. Part 1 (Rappoport, Z., Ed.) pp 255−305, John Wiley & Sons, Chichester, U.K.
18. Yao, M., Ose, T., Sugimoto, H., Horiuchi, A., Nakagawa, A., Wakatsuki, S., Yokoi, S., Murakami, T., Honma, M., and Tanaka, I. (2000) Crystal structure of 1-aminocyclopropane-1-carboxylate deaminase from *Hansenula saturnus*. *J. Biol. Chem. 275*, 34557–34565.
19. Ose, T., Fujino, A., Yao, M., Watanabe, N., Honma, M., and Tanaka, I. (2003) Reaction intermediate structures of 1-aminocyclopropane-1-carboxylate deaminase: Insight into PLP-dependent cyclopropane ring-opening reaction. *J. Biol. Chem. 278*, 41069–41076.
20. Karthikeyan, S., Zhao, Z., Kao, C.-L., Zhou, Q., Tao, Z., Zhang, H., and Liu, H.-w. (2004) Structural analysis of 1-aminocyclopropane-1-carboxylate deaminase: Observation of an aminyl intermediate and identification of Tyr 294 as the active-site nucleophile. *Angew. Chem., Int. Ed. 43*, 3425–3429.
21. Karthikeyan, S., Zhou, Q., Zhao, Z., Kao, C.-L., Tao, Z., Robinson, H., Liu, H.-w., and Zhang, H. (2004) Structural analysis of *Pseudomonas* 1-aminocyclopropane-1-carboxylate deaminase complexes: Insight into the mechanism of a unique pyridoxal-5′-phosphate dependent cyclopropane ring-opening reaction. *Biochemistry 43*, 13328–13339.
22. Zhao, Z., Chen, H., Li, K., Du, W., He, S., and Liu, H.-w. (2003) Reaction of 1-amino-2-methylenecyclopropane-1-carboxylate with 1-aminocyclopropane-1-carboxylate deaminase: Analysis and mechanistic implications. *Biochemistry 42*, 2089–2103.
23. Thibblin, A., and Jencks, W. P. (1979) Unstable carbanions. General acid catalysis of the cleavage of 1-phenylcyclopropanol and 1-phenyl-2-arylcyclopropanol anions. *J. Am. Chem. Soc. 101*, 4963–4973.
24. Wiberg, K. B., and Kass, S. R. (1985) Electrophilic cleavage of cyclopropanes. Acetolysis of alkylcyclopropanes. *J. Am. Chem. Soc. 107*, 988–995.
25. Baird, R. L., and Aboderin, A. A. (1964) Concerning the role of protonated cyclopropane intermediates in solvolytic reactions. The solvolysis of cyclopropane in deuteriosulfuric acid. *J. Am. Chem. Soc. 86*, 252–255.
26. McKinney, M. A., Smith, S. H., Hempelman, S., Gearen, M. M., and Pearson, L. (1971) Proteolytic cleavage of cyclopropanes: The structure of the transition state in the protonation of arylcyclopropanes. *Tetrahedron Lett.*, 3657–3660.
27. McKinney, M. A., and So, E. C. (1972) Protolytic cleavage of cyclopropanes. The two mechanisms for the acid-catalyzed cleavage of 1-phenylcyclopropylmethyl ether. *J. Org. Chem. 37*, 2818–2822.
28. Bradford, M. M. (1976) A rapid and sensitive method for the quantitation of microgram quantities of protein utilizing the principle of protein-dye binding. *Anal. Biochem. 72*, 248–254.
29. St. Maurice, M., and Bearne, S. L. (2002) Kinetics and thermodynamics of mandelate racemase catalysis. *Biochemistry 41*, 4048–4058.
30. Schowen, K. B., and Schowen, R. L. (1982) Solvent isotope effects on enzyme systems. *Methods Enzymol. 87*, 551–606.
31. Singleton, D. A., and Thomas, A. A. (1995) High-precision simultaneous determination of multiple small kinetic isotope effects at natural abundance. *J. Am. Chem. Soc. 117*, 9357–9358.
32. Northrop, D. B. (1975) Steady-state analysis of kinetic isotope effects in enzymic reactions. *Biochemistry 14*, 2644–2651.
33. Simon, H., and Palm, D. (1966) Isotope effects in organic chemistry and biochemistry. *Angew. Chem., Int. Ed. 5*, 920–933.
34. Cleland, W. W. (2005) The use of isotope effects to determine enzyme mechanisms. *Arch. Biochem. Biophys. 433*, 2–12.
35. Bigeleisen, J., and Wolfsberg, M. (1958) Theoretical and experimental aspects of isotope effects in chemical kinetics. *Adv. Chem. Phys. 1*, 15–76.
36. Yano, T., Kuramitsu, S., Tanase, S., Morino, Y., and Kagamiyama, H. (1992) Role of Asp222 in the catalytic mechanism of *Escherichia coli* aspartate aminotransferase: The amino acid residue which enhances the function of the enzyme-bound coenzyme pyridoxal 5′-phosphate. *Biochemistry 31*, 5878–5887.
37. Yano, T., Hinoue, Y., Chen, V. J., Metzler, D. E., Miyahara, I., Hirotsu, K., and Kagamiyama, H. (1993) Role of an active site residue

analyzed by combination of mutagenesis and coenzyme analog. *J. Mol. Biol. 234*, 1218–1229.
38. Gong, J., Hunter, G. A., and Ferreira, G. C. (1998) Aspartate-279 in aminolevulinate synthase affects enzyme catalysis through enhancing the function of the pyridoxal 5′-phosphate cofactor. *Biochemistry 37*, 3509–3517.
39. Momany, C., Levdikov, V., Blagova, L., Lima, S., and Phillips, R. S. (2004) Three-dimensional structure of kynureninase from *Pseudomonas fluorescens*. *Biochemistry 43*, 1193–1203.
40. Morozov, Y. V. (1986) Spectroscopic properties, electronic structure, and photochemical behavior of vitamin B_6 and analogs. In Vitamine B6 pyridoxal phosphate: Chemical, biochemical, and medical aspects (Dolphin, D., Poulson, R., and Avramovic, O., Eds.) Part A, pp 131−222, John Wiley & Sons, New York.
41. Eliot, A. C., and Kirsch, J. F. (2002) Modulation of the internal aldimine pK_a's of 1-aminocyclopropane-1-carboxylate synthase and aspartate aminotransferase by specific active site residues. *Biochemistry 41*, 3836–3842.
42. Li, Y., Feng, L., and Kirsch, J. F. (1997) Kinetic and spectroscopic investigations of wild-type and mutant forms of apple 1-aminocyclopropane-1-carboxylate synthase. *Biochemistry 36*, 15477–15488.
43. Zhou, X., and Toney, M. D. (1999) pH studies on the mechanism of the pyridoxal phosphate-dependent dialkylglycine decarboxylase. *Biochemistry 38*, 311–320.
44. Osterman, A. L., Brooks, H. B., Rizo, J., and Phillips, M. A. (1997) Role of Arg-277 in the binding of pyridoxal 5′-phosphate to *Trypanosoma brucei* ornithine decarboxylase. *Biochemistry 36*, 4558–4567.
45. Hayashi, H., Mizuguchi, H., and Kagamiyama, H. (1993) Rat liver aromatic L-amino acid decarboxylase: Spectroscopic and kinetic analysis of the coenzyme and reaction intermediates. *Biochemistry 32*, 812–818.
46. Metzler, C. M., Viswanath, R., and Metzler, D. E. (1991) Equilibria and absorption spectra of tryptophanase. *J. Biol. Chem. 266*, 9374–9381.
47. Karsten, W. E., Ohshiro, T., Izumi, Y., and Cook, P. F. (2005) Reaction of serine-glyoxylate aminotransferase with the alternative substrate ketomalonate indicates rate-limiting protonation of a quinonoid intermediate. *Biochemistry 44*, 15930–15936.
48. Karsten, W. E., Ohshiro, T., Izumi, Y., and Cook, P. F. (2001) Initial velocity, spectral, and pH studies of the serine-glyoxylate aminotransferase from *Hyphomicrobium methylovorum*. *Arch. Biochem. Biophys. 388*, 267–275.
49. Grinnell, J., and Fornwalt, H. J. (1936) The viscosity of deuterium oxide and its mixtures with water at 25 °C. *J. Chem. Phys. 4*, 30–33.
50. Cerjan, C., and Barnett, R. E. (1972) Viscosity dependence of a putative diffusion-limited reaction. *J. Phys. Chem. 76*, 1192–1195.
51. Nakatani, H., and Dunford, H. B. (1979) Meaning of diffusion-controlled association rate constants in enzymology. *J. Phys. Chem. 83*, 2662–2665.
52. Brouwer, A. C., and Kirsch, J. F. (1982) Investigation of diffusion-limited rates of chymotrypsin reactions by viscosity variation. *Biochemistry 21*, 1302–1307.
53. Hardy, L. W., and Kirsch, J. F. (1984) Diffusion-limited component of reactions catalyzed by *Bacillus cereus* β-lactamase. *Biochemistry 23*, 1275–1282.
54. Kurz, L. C., Weitkamp, E., and Frieden, C. (1987) Adenosine deaminase: Viscosity studies and the mechanism of binding of substrate and of ground- and transition-state analogue inhibitors. *Biochemistry 26*, 3027–3032.
55. Adams, J. A., and Taylor, S. S. (1992) Energetic limits of phosphotransfer in the catalytic subunit of cAMP dependent protein kinase as measured by viscosity experiments. *Biochemistry 31*, 8516–8522.
56. Wood, B. M., Chan, K. K., Amyes, T. L., Richard, J. P., and Gerlt, J. A. (2009) Mechanism of the orotidine 5′-monophosphate decarboxylase-catalyzed reaction: Effect of solvent viscosity on kinetic constants. *Biochemistry 48*, 5510.
57. Raber, M. L., Freeman, M. F., and Townsend, C. A. (2009) Dissection of the stepwise mechanism to β-lactam formation and elucidation of a rate-determining conformational change in β-lactam synthetase. *J. Biol. Chem. 284*, 207–217.
58. Francis, K., and Gadda, G. (2006) Probing the chemical steps of nitroalkane oxidation catalyzed by 2 nitropropane dioxygenase with solvent viscosity, pH, and substrate kinetic isotope effects. *Biochemistry 45*, 13889–13898.
59. Scharschmidt, M., Fisher, M. A., and Cleland, W. W. (1984) Variation of transition-state structure as a function of the nucleotide in reactions catalyzed by dehydrogenases. 1. Liver alcohol dehydrogenase with benzyl alcohol and yeast aldehyde dehydrogenase with benzaldehyde. *Biochemistry 23*, 5471–5478.
60. Hess, R. A., Hengge, A. C., and Cleland, W. W. (1998) Isotope effects on enzyme-catalyzed acyl transfer from p-nitrophenyl acetate: Concerted mechanisms and increased hyperconjugation in the transition state. *J. Am. Chem. Soc. 120*, 2703–2709.
61. Lee, J. K., Bain, A. D., and Berti, P. J. (2004) Probing the transition states of four glucoside hydrolyses with ^{13}C kinetic isotope effects measured at natural abundance by NMR spectroscopy. *J. Am. Chem. Soc. 126*, 3769–3776.
62. Swanson, T., Brooks, H. B., Osterman, A. L., O'Leary, M. H., and Phillips, M. A. (1998) Carbon-13 isotope effect studies of *Trypanosoma brucei* ornithine decarboxylase. *Biochemistry 37*, 14943–14947.
63. O'Leary, M. H. (1988) Transition-state structures in enzyme-catalyzed decarboxylations. *Acc. Chem. Res. 21*, 450–455.
64. O'Leary, M. H., Richards, D. T., and Hendrickson, D. W. (1970) Carbon isotope effects on the enzymic decarboxylation of glutamic acid. *J. Am. Chem. Soc. 92*, 4435–4440.
65. Erion, M. D., and Walsh, C. T. (1987) 1-Aminocyclopropanephosphonate: Time-dependent inactivation of 1-aminocyclopropanecarboxylate deaminase and *Bacillus stearothermophilus* alanine racemase by slow dissociation behavior. *Biochemistry 26*, 3417–3425.
66. Woehl, E. U., Tai, C.-H., Dunn, M. F., and Cook, P. F. (1996) Formation of the α-aminoacrylate intermediate limits the overall reaction catalyzed by *O*-acetylserine sulfhydrylase. *Biochemistry 35*, 4776–4783.
67. Tidwell, T. T. (1987) Conjugative and substitutive properties of the cyclopropyl group. In The chemistry of the cyclopropyl group (Rappoport, Z., Ed.) Vol. 1, pp 565−632, John Wiley & Sons, New York.
68. Kortemme, T., and Creighton, T. E. (1995) Ionization of cysteine residues at the termini of model α-helical peptides. Relevance to unusual thiol pK_a values in proteins of the thioredoxin family. *J. Mol. Biol. 253*, 799–812.
69. Davies, C., Heath, R. J., White, S. W., and Rock, C. O. (2000) The 1.8 Å crystal structure and active-site architecture of β-ketoacyl-acyl carrier protein synthase III (FabH) from *Escherichia coli*. *Structure 8*, 185–195.
70. Snook, C. F., Tipton, P. A., and Beamer, L. J. (2003) Crystal structure of GDP-mannose dehydrogenase: A key enzyme of alginate biosynthesis in *P. aeruginosa*. *Biochemistry 42*, 4658–4668.
71. Anderson, V. E., Ruszczycky, M. W., and Harris, M. E. (2006) Activation of oxygen nucleophiles in enzyme catalysis. *Chem. Rev. 106*, 3236–3251.
72. Brzovic, P., Holbrook, E. L., Greene, R. C., and Dunn, M. F. (1990) Reaction mechanism of *Escherichia coli* cystathionine γ-synthase: Direct evidence for a pyridoxamine derivative of vinylglyoxylate as a key intermediate in pyridoxal phosphate dependent γ-elimination and γ-replacement reactions. *Biochemistry 29*, 442–451.